

Frederico M. A. Silva

silvafma@eec.ufg.br
Federal University of Goiás
Civil Engineering Department
74605-220 Goiânia, Goiás, Brazil

Paulo B. Gonçalves

paulo@puc-rio.br
Pontifical Catholic University of Rio de Janeiro
Civil Engineering Department
22453-900 Rio de Janeiro, RJ, Brazil

Zenón J. G. N. Del Prado

zenon@eec.ufg.br
Federal University of Goiás
Civil Engineering Department
74605-220 Goiânia, Goiás, Brazil

Influence of Physical and Geometrical System Parameters Uncertainties on the Nonlinear Oscillations of Cylindrical Shells

This work investigates the influence of physical and geometrical system parameters uncertainties and excitation noise on the nonlinear vibrations and stability of simply-supported cylindrical shells. These parameters are composed of both deterministic and random terms. Donnell's non-linear shallow shell theory is used to study the non-linear vibrations of the shell. To discretize the partial differential equations of motion, first, a general expression for the transversal displacement is obtained by a perturbation procedure which identifies all modes that couple with the linear modes through the quadratic and cubic nonlinearities. Then, a particular solution is selected which ensures the convergence of the response up to very large deflections. Finally, the in-plane displacements are obtained as a function of the transversal displacement by solving the in-plane equations analytically and imposing the necessary boundary, continuity and symmetry conditions. Substituting the obtained modal expansions into the equation of motion and applying the Galerkin's method, a discrete system in time domain is obtained. Several numerical strategies are used to study the nonlinear behavior of the shell considering the uncertainties in the physical and geometrical system parameters. Special attention is given to the influence of the uncertainties on the parametric instability and escape boundaries.

Keywords: dynamic instability, uncertainties, nonlinear analysis, cylindrical shells

Introduction

Cylindrical shells are one of the most common structural elements with applications in nearly all engineering fields. They are particularly suited to withstand axial loads and lateral pressure. Under these loading conditions thin-walled cylindrical shells usually display a complex nonlinear response due to modal coupling and interaction and high imperfection sensitivity. The study of the nonlinear vibrations of cylindrical shells goes back to the middle of the last century with the works by Chu (1961), Nowinski (1963), Evensen (1963, 1967) and Olson (1965), among others. In these works either the Ritz or Galerkin method are used to discretize the shell. For this, a modal expansion for the displacement field is necessary. The development of consistent modal solutions capable of describing the main modal interactions observed in cylindrical shells has received much attention in literature. A detailed review of this subject was published in 2003 by Amabili and Paidoussis (2003).

Also, a considerable effort in structural engineering has been directed towards understanding the behavior of structures liable to buckling (Bazant and Cedolin, 1991). This step is essential for the development of safe design criteria (Ziemian, 2010). While a good correlation between the experimental results and the theoretical critical loads can be observed for structural elements exhibiting stable post-buckling behavior, such as plates and columns, a persistent discrepancy between theoretical and experimental buckling loads is observed for structural systems exhibiting unstable post-buckling behavior, being the experimental results lower than the theoretical ones. Figure 1 compares the normalized theoretical critical load of a perfect cylindrical shell under axial load with the scatter of experimental results found in the literature (Batista and Gonçalves, 1994). Here (R/h) is the radius-to-thickness ratio, which is a measure of the shell slenderness. The experimental results are much lower than the theoretical critical load, being the theoretical value a distant upper bound. This is an archetypal example of an imperfection sensitive structure in structural stability.

A general explanation for this upsetting behavior was given by Koiter in his pioneering work on the general theory of buckling and post-buckling behavior of elastic structures (Koiter, 1945; Kounadis, 2006). Koiter showed that imperfections in the geometry or in the load may decrease substantially the load carrying capacity of these structures under slow variation of the applied load. However these imperfections are not known a priori and may even change during the service life of the structure. In addition, load imperfections may cause a further decrease in the critical load. This scenario becomes even worse if the unavoidable uncertainties in system parameters are also taken into account. Since the expressions for the critical load are developed based on a static equilibrium analysis, they actually calculate an upper bound for the load carrying capacity of the real structure, as they do not take into account the disturbances imposed upon the imperfect structure during its service life (Santee, 1999). The influence of these disturbances on the integrity of the structure can be evaluated by analyzing the evolution of the basins of attraction of the stable equilibrium configurations as a function of the system parameters. This issue was first addressed by Thompson and co-workers (Thompson, 1989; Soliman and Thompson, 1989, 1992). They introduced the concepts of safe basin and erosion profiles. It was

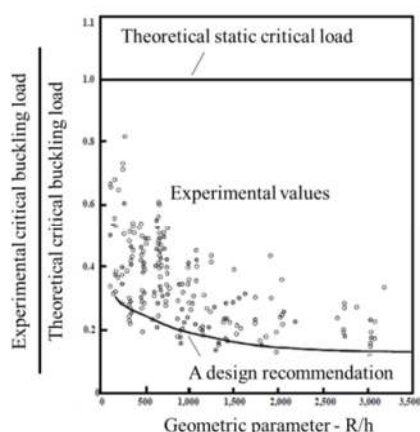


Figure 1. Comparison of the theoretical critical load of a cylindrical shell under axial load with the scatter of experimental results.

Paper received 17 April 2012. Paper accepted 3 September 2012.

further analyzed by several authors and nowadays it is agreed that the safety of a nonlinear mechanical system or structure depends not only on the stability of their solutions, but also on the continuous and uncorrupted basin surrounding each solution, the total erosion of a given basin corresponding to the system failure. The integrity of a basin of attraction depends on the topology of the basin boundary, which can be smooth or fractal, and on the way that the basins of the various co-existing solutions interfere with each other. This topic is particularly important in systems exhibiting multiple potential well, where the basins of various in-well and cross-well solutions are intertwined. In a recent work Rega and Lenci (2005) summarized the current knowledge in the area and introduced new concepts which can be efficiently used for the integrity analysis of nonlinear systems. Recently, using these concepts, Gonçalves et al. (2011) studied the global dynamics and topological integrity of the basins of attraction of a parametrically excited cylindrical shell through a two-degree-of-freedom reduced order model. However the investigation of the influence of uncertainties and random noise on the evolution and stratification of the basins of attraction must also be carried out to arrive at a safe load level for design.

To take indirectly into account these deleterious effects, several lower bounds of static buckling loads have been proposed for design. They are usually based on the scatter of experimental buckling loads and energy considerations (Batista and Gonçalves, 1994). Estimate of the dynamic buckling load of structures with unstable post-buckling behavior – the load corresponding to escape from the safe pre-buckling well – considering the effects of uncertainties and imperfections is a much more difficult task. Structures under dynamic loads may exhibit both local and global bifurcations that affect in different ways the load carrying capacity and degree of safety of the structure. Global bifurcations are particularly important since they control, as shown by Soliman and Thompson (1989), the evolution of the basins of attraction of the solutions in phase space. In addition, compared with the static case, the number of load control parameters is higher. Finally, experimental results of dynamic buckling loads of slender structures are rather scarce in literature (Virgin, 2000; Amabili, 2008). Therefore, little is known on the effects of uncertainties on the load carrying capacity of structures liable to unstable static buckling in a dynamic environment. In a recent work Gonçalves and Santee (2008) analyzed the influence of uncertainties on the load carrying capacity of a simplified structural model exhibiting unstable post-buckling behavior. Using several tools of non-linear dynamics, they showed that the uncertainties have an influence similar and of the same order as geometric imperfections on the scatter of buckling loads and proposed a safe lower bound based on Melnikov's criterion. Thus, the aim of the present work is, using a similar methodology, to study the influence of uncertainties on the dynamic stability of a cylindrical shell under axial loads.

The influence of combined random material and geometric properties on the free vibration frequencies and buckling loads of cylindrical shells has been investigated by, among others, Yadav and Verma (2001); Singh, Yadav and Iyengar (2002); Stefanou and Papadarakakis (2004); Papadopoulos and Papadarakakis (2005); Kriegesmann et al. (2010) and Stefanou (2011). On the other hand, there is a lack of information on the influence of these uncertainties on the post-buckling behavior and particularly on the nonlinear oscillations of these structures. However, for other systems, a number of publications, in recent years, have investigated the influence of random noise on their bifurcations, basins of attraction and the competition between different attractors (Lai and Winslow, 1994; Kraut, Feudel, and Grebogi, 1999; Kraut and Feudel, 2002). As an extension of these previous works, and following the methodology described in Gonçalves, Silva and Del Prado (2008) for the derivation of consistent reduced order models for the

nonlinear vibrations of cylindrical shells, the present work investigates the influence of small uncertainties in the physical and geometrical parameters of the shell and the unavoidable noise present in the axial excitation on the dynamic buckling loads and bifurcation diagrams. For this, a detailed parametric analysis is carried out to clarify the influence of uncertainties in load and system parameters.

Nomenclature

D	= flexural stiffness of the shell, $N.m$
E	= Young's modulus, Pa
$G(P_1, \omega, t)$	= random disturbance in axial load, N/m
h	= thickness, m
L	= length, m
m, n	= number of longitudinal half-waves and circumferential waves, respectively
$M_x, M_\theta, M_{x\theta}$	= moments resultants in, respectively, axial, circumferential and in-plane direction, $N.m/m$
$N_x, N_\theta, N_{x\theta}$	= force resultants in, respectively, axial, circumferential and in-plane direction, N/m
P_0	= axial static pre-load, N/m
P_1	= amplitude of the deterministic harmonic axial load, N/m
P_{cr}	= classical axial buckling load, N/m
Q	= parameter which expresses the quality of the fabrication process
R	= radius, m
t	= time, s
u, v, w	= axial, circumferential and transversal displacements of shell's middle surface, m
x	= axial coordinate, m
W	= non-dimensional parameter for transversal displacements
z	= transversal coordinate, m

Greek Symbols

α	= system parameter (E, ν, ρ, L, R or h)
α_0	= mean value of the chosen parameter (design value)
δ	= standard deviation parameter
ε	= non-dimensional parameter for axial coordinate
Γ_0	= non-dimensional parameter for axial static pre-load
Γ_1	= non-dimensional parameter for amplitude of the deterministic harmonic axial load
η_1, η_2	= linear viscous and viscoelastic material damping coefficient
ν	= Poisson's coefficient
θ	= circumferential coordinate, rad
ρ	= mass density, kg/m^3
$\bar{\sigma}_x, \bar{\sigma}_\theta$	= stresses at an arbitrary point of shell in, respectively, axial and circumferential direction
σ_{GG}^2	= variance of the random force amplitude
$\bar{\tau}_{x\theta}$	= tangential resultant stresses at an arbitrary point of shell
τ	= non-dimensional parameter for time
ω	= deterministic excitation frequency, rad/s
ω_0	= lowest vibration frequency of the shell for nominal values of physical and geometrical parameters, rad/s
ω_1	= frequency bandwidth of the excitation frequency, rad/s
Ω	= non-dimensional parameter for deterministic excitation frequency

Problem Formulation

Shell equation

Consider a cylindrical shell of radius R , thickness h and length L , made of a linear elastic material with Young's modulus E , Poisson coefficient ν and mass density ρ . For an isotropic shell the stresses at an arbitrary point are given in terms of the middle surface strains and changes of curvature, according to Donnell's shallow shell theory, by:

$$\begin{Bmatrix} \bar{\sigma}_x \\ \bar{\sigma}_\theta \\ \bar{\tau}_{x\theta} \end{Bmatrix} = \frac{E}{(1-\nu^2)} \begin{bmatrix} 1 & \nu & 0 \\ \nu & 1 & 0 \\ 0 & 0 & \frac{(1-\nu)}{2} \end{bmatrix} \begin{Bmatrix} u_{,x} + \frac{1}{2} w_{,x}^2 - z w_{,xx} \\ \frac{1}{R} (v_{,\theta} + w) - \frac{z}{R^2} w_{,\theta\theta} \\ v_{,x} + \frac{1}{R} (u_{,\theta} + w_{,x} w_{,\theta}) - \frac{2z}{R} w_{,x\theta} \end{Bmatrix} \quad (1)$$

The shell is subjected to a harmonic axial load of the form:

$$P = P_0 + P_1 \cos(\omega t) + G(P_1, \omega, t) \quad (2)$$

where P_0 is the axial static pre-load, P_1 is the amplitude of the deterministic harmonic load, ω is the deterministic excitation frequency, t is time and $G(P_1, \omega, t)$ is the random disturbance that depends on the deterministic parameters P_1 and ω .

The nonlinear equations of motion, considering only the transversal inertia and damping forces, are given in terms of the force and moments resultants as:

$$N_{x,x} + \frac{N_{x\theta,\theta}}{R} = 0 \quad (3)$$

$$N_{x\theta,x} + \frac{N_{\theta,\theta}}{R} = 0 \quad (4)$$

$$\begin{aligned} & \rho h \ddot{w} + 2\eta_1 \rho \omega_0 h \dot{w} + \eta_2 D \nabla^4 \dot{w} - \frac{1}{R^2} \left[\frac{M_{\theta,\theta\theta}}{R} \right. \\ & + 2M_{x\theta,x\theta} + R M_{x,xx} + R(N_x - P) + \\ & \left. N_\theta \left(\frac{w_{,\theta\theta}}{R} - 1 \right) + 2N_{x\theta} w_{,x\theta} \right] = 0 \end{aligned} \quad (5)$$

where η_1 and η_2 are, respectively, the linear viscous damping and the viscoelastic material damping coefficients, $D = Eh^3/12(1-\nu^2)$ is the flexural stiffness of the shell, ω_0 is the lowest vibration frequency of the shell for nominal values of physical and geometrical parameters and the force and moments' resultants are obtained by the integration of the stress components along the shell thickness as follows:

$$\begin{aligned} [N_x, N_\theta, N_{x\theta}] &= \int_{-h/2}^{h/2} [\bar{\sigma}_x, \bar{\sigma}_\theta, \bar{\tau}_{x\theta}] dz \\ [M_x, M_\theta, M_{x\theta}] &= \int_{-h/2}^{h/2} [z \bar{\sigma}_x, z \bar{\sigma}_\theta, z \bar{\tau}_{x\theta}] dz \end{aligned} \quad (6)$$

For a simply-supported shell, the following boundary conditions must be satisfied:

$$v(0, \theta) = v(L, \theta) = 0 \quad (7)$$

$$w(0, \theta) = w(L, \theta) = 0 \quad (8)$$

$$M_x(0, \theta) = M_x(L, \theta) = 0 \quad (9)$$

$$N_x(0, \theta) = N_x(L, \theta) = 0 \quad (10)$$

The boundary condition, Eq. (10), is a nonlinear boundary condition when written in terms of the displacements, that is:

$$N_x = \frac{Eh}{1-\nu^2} \left[u_{,x} + \frac{1}{2} w_{,x}^2 + \frac{\nu}{R} \left(v_{,\theta} + w + \frac{1}{2R} w_{,\theta}^2 \right) \right] \quad (11)$$

The displacement field, in this work, is also required to satisfy the following conditions:

$$u(L/2, \theta) = 0 \quad \text{and} \quad v(x, 0) = v(x, 2\pi) \quad (12)$$

The symmetry of the axial displacement field is a consequence of the adopted modal solution for the transversal displacement field and the symmetry of the boundary conditions (Eqs. (7)-(10)). In the foregoing, the following non-dimensional parameters have been introduced:

$$\begin{aligned} W &= \frac{w}{h} & \varepsilon &= \frac{x}{L} & \tau &= \omega_0 t & \Omega &= \frac{\omega}{\omega_0} \\ \Gamma_0 &= \frac{P_0}{P_{cr}} & \Gamma_1 &= \frac{P_1}{P_{cr}} & P_{cr} &= \frac{Eh^2}{R\sqrt{3(1-\nu^2)}} \end{aligned} \quad (13)$$

Here P_{cr} is the classical axial buckling load of the shell.

General solution of the shell displacement field by a perturbation procedure

The numerical model is developed by expanding the transversal displacement component w in series in the circumferential and axial variables. From previous investigations on modal solutions for the nonlinear analysis of cylindrical shells under axial loads (Gonçalves and Batista, 1988; Gonçalves and Del Prado, 2002, 2005), it is observed that, in order to obtain a consistent modeling with a limited number of modes, the sum of shape functions for the displacements must express the nonlinear coupling between the modes and describe consistently the unstable post-buckling response of the shell as well as the correct frequency-amplitude relation.

Based on a perturbation procedure, the lateral deflection w can be described as:

$$\begin{aligned} W &= \sum_{i=1,3,5} \sum_{j=1,3,5} \zeta_{ij}(\tau) \cos(in\theta) \sin(jm\pi\xi) \\ &+ \sum_{k=0,2,4} \sum_{l=0,2,4} \zeta_{kl}(\tau) \cos(kn\theta) \cos(lm\pi\xi) \end{aligned} \quad (14)$$

By imposing the boundary conditions, Eq. (8) and Eq. (9), and by retaining in Eq. (14) the number of modes necessary to achieve convergence up to very large deflections, one obtains for the transversal displacement (Gonçalves, Silva and Del Prado, 2008; Silva, Gonçalves and Del Prado, 2011):

$$\begin{aligned}
 W = & \left[\zeta_{11}(\tau) \cos(n\theta) + \zeta_{31}(\tau) \cos(3n\theta) \right] \sin(m\pi \varepsilon) \\
 & + \left[\zeta_{13}(\tau) \cos(n\theta) + \zeta_{33}(\tau) \cos(3n\theta) \right] \sin(3m\pi \varepsilon) \\
 & + \left[\zeta_{02}(\tau) + \zeta_{22}(\tau) \cos(2n\theta) \right] \\
 & \left[-\frac{3}{4} + \cos(2m\pi \varepsilon) - \frac{1}{4} \cos(4m\pi \varepsilon) \right]
 \end{aligned} \tag{15}$$

The in-plane displacements u and v are obtained by substituting Eq. (15) into the in-plane equilibrium equations, Eq. (3) and Eq. (4), and by solving the system of linear partial differential equations in u and v and imposing the relevant boundary, symmetry and continuity conditions. Based on this procedure one obtains the necessary number of in-plane modes and writes their modal amplitudes in terms of the modal amplitudes $\zeta_{ij}(t)$ in Eq. (15) (Gonçalves, Silva and Del Prado, 2008; Silva, Gonçalves and Del Prado, 2011). Finally, by substituting the adopted expansion for the transversal displacement w together with the obtained expressions for u and v into the equation of motion in the transversal direction, Eq. (5), and by applying the standard Galerkin method, a consistent discretized system of ordinary differential equations of motion is derived.

Simulation of the uncertainties in the physical and geometric parameters

The physical parameters (E , ν and ρ) and the geometrical parameters (L , R and h) of the shell usually have some reference values which are defined at the stage of design. However, depending on the allowable tolerances in the fabrication process, small variations of these parameters may occur. Usually these small variations have a negligible influence on the load capacity of the structure. But in structural systems liable to buckling, due mainly to the inherent nonlinearity of the buckling process, small changes may lead to significant changes in the load capacity and safety of the structure.

For each physical and geometrical parameter, α , the following uniform probability density function, f , is assumed (Gonçalves and Santee, 2008):

$$f(\alpha) = \begin{cases} \frac{100}{2\alpha_0 Q}, & \text{if } \alpha_0 - \frac{\alpha_0 Q}{100} < \alpha < \alpha_0 + \frac{\alpha_0 Q}{100} \\ 0, & \text{otherwise} \end{cases} \tag{16}$$

where α is the system parameter (E , ν , ρ , L , R or h), α_0 is the mean value of the chosen parameter (design value), and Q is a parameter which expresses the quality of the fabrication process as a percentage of the mean value, α_0 .

Simulation of the random force

For the numerical calculations of the present work, the non-deterministic term of the axial load in Eq. (2), $G(P_1, \omega, t)$, is considered as a stationary and ergodic continuous stochastic process in time (Gonçalves and Santee, 2008). Another hypothesis is that the stochastic process $G(P_1, \omega, t)$ has a zero expected value, that is:

$$E[G(P_1, \omega, t)] = 0 \tag{17}$$

The description of a stochastic process is usually made in the frequency domain. Here, it is assumed that the random term $G(P_1, \omega, t)$ has a spectral density function given by:

$$\Phi_{GG}(\bar{\omega}) = \frac{\sigma_{GG}^2}{2\omega_l} \text{ for } \Omega - \frac{\omega_l}{2} < \bar{\omega} < \Omega + \frac{\omega_l}{2} \tag{18}$$

where σ_{GG}^2 is the variance of the random force amplitude and ω_l is the frequency bandwidth of the excitation frequency.

Additionally, it is considered that the standard deviation of the random force amplitude is proportional to the deterministic force amplitude, P_1 , thus:

$$\sigma_{GG} = \delta P_1 \tag{19}$$

where δ is the standard deviation parameter of proportionality. So, the random force is a stochastic process that depends on the frequency, ω , and amplitude, P_1 , of the deterministic term. The numerical algorithms used in the present work can be found in Gonçalves and Santee (2008).

Numerical Results

Consider a cylindrical shell of radius $R = 0.2$ m, length $L = 0.4$ m and thickness $h = 0.002$ m. The shell material has the following properties: $E = 210$ GPa, $\nu = 0.3$ and $\rho = 7850$ kg/m³. For this shell geometry the lowest buckling load as well as the lowest natural frequency are obtained for $m = 1$ and $n = 5$ (Gonçalves and Del Prado, 2005). The viscous and material damping coefficients, η_1 and η_2 , are, respectively, 0.0008 and 0.0001. These values will be used throughout the present numerical analysis. These values are based on the experimental results by Amabili and co-workers (Amabili, 2008).

Numerical results with physical and geometrical uncertainties

The continuous black curves in Figs. 2 and 3 are the parametric and permanent escape boundaries in the force control space, considering a deterministic harmonic axial load in Eq. (2) ($G(P_1, \omega, t) = 0$). The dashed horizontal line represents the critical static axial load, $\Gamma_{cr} = \Gamma_0 + \Gamma_1$. The dashed vertical lines identify the lowest natural frequency of the shell and twice this value, which corresponds to the main parametric resonance region. The region below the parametric instability boundary corresponds to sets of load parameters (frequency/forcing amplitude) that lead to stable trivial solutions, that is, under small perturbations the perturbed response tends to zero as time increases. The region above the escape boundary corresponds to force parameters that lead to escape from the pre-buckling well. After escape, the shell may exhibit small amplitude oscillations around a post-buckling equilibrium position or large cross-well motions. Between these two regions, there is a region with a complex dynamics where, depending on the initial conditions, the shell may display harmonic or sub-harmonic motions within the pre-buckling well or escape from the pre-buckling well. In this region, the dynamic response and, consequently, the dynamic buckling load are rather sensitive to physical and geometrical uncertainties.

Figures 2 and 3 show the influence of the uncertainty in the Young modulus E and in shell thickness h on the parametric instability and escape boundaries in the force control space. In these figures, the curves in gray are derived from the analysis of ten samples randomly generated within the range of the quality parameter (Q) in Eq. (16).

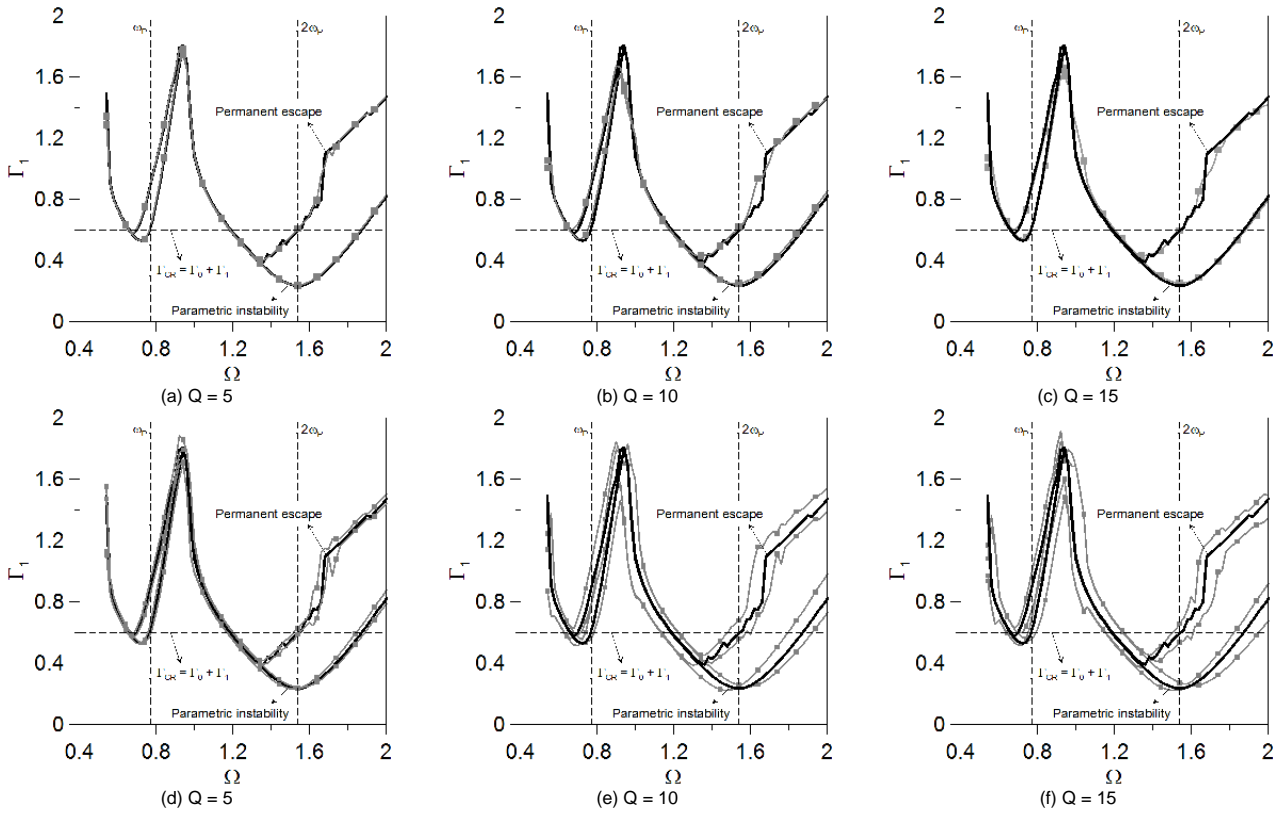


Figure 2. Parametric and escape instability boundaries in the force control space, considering an uncertainty in the Young modulus, E . ($\Gamma_0 = 0.40$, $G(P_i, \omega, \eta) = 0$).

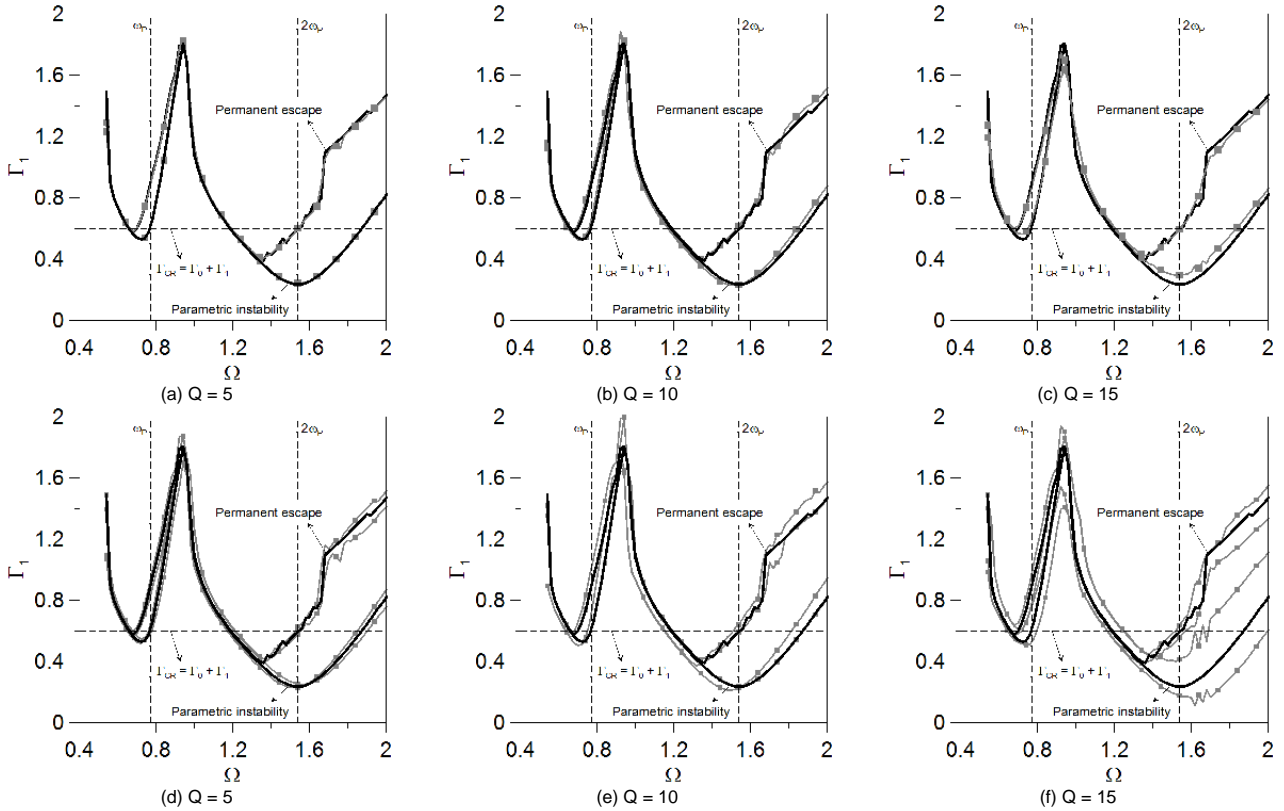


Figure 3. Parametric and escape instability boundaries in the force control space, considering an uncertainty in the shell thickness, h . ($\Gamma_0 = 0.40$, $G(P_i, \omega, \eta) = 0$).

The curves in gray in Figs. 2a-c and 3a-c represent, respectively, the mean parametric instability boundary and escape boundary, obtained using the arithmetic mean value of the ten critical loads. The curves in gray in Figs. 2d-f and 3d-f illustrate, respectively, the parametric and escape instability boundaries considering the average value plus or minus the standard deviation of ten samples.

The stability boundaries shown in Figs. 2a-c and 3a-c obtained by the mean value of the critical loads are slightly different from those obtained for the reference system. This difference increases with the value of Q . In all cases the upper and lower bounds of the ten samples, as shown in Figs. 2f and 3f, lead to a high variability of the critical loads, especially on the right hand side of the main parametric instability region where the parametric instability is characterized by a super-critical bifurcation leading to a period two solution. The critical load is particularly sensitive to the small variations in the shell thickness, as expected for a thin-walled structure.

Figure 4 illustrates the possible types of the shell response in the vicinity of each stability boundary shown in Fig. 2 through time responses, projections of the phase space and Poincaré sections (dots along the phase space projections). If the cylinder is subjected to a periodic axial load, it will undergo the familiar longitudinal forced vibration, exhibiting a uniform transversal motion, due to the effect of

Poisson's ration, also known as breathing mode. However at certain critical values, the longitudinal motion becomes unstable and the cylinder executes transverse bending vibrations. In Fig. 4a, for a forcing amplitude lower than the critical value ($\Gamma_I = 0.60$) and $\Omega = 1.20$, after a small initial disturbance, the amplitude of the response decreases rapidly converging to the trivial solution. If the control parameter Γ_I is increased slightly beyond the critical value, ($\Gamma_I = 0.65$), the shell exhibits initially an exponential growth of the amplitude, as predicted by the linear theory, converging to a limit cycle within the pre-buckling well. In this case the trivial solution becomes unstable and the system converges to a period-two stable solution (a period- k response means a steady state response with a period k times that of the forcing). Figure 4b illustrates the shell response in the vicinity of the escape boundary. For $\Gamma_I = 0.60$ and $\Omega = 1.60$ the response converges to a limit cycle of period two within the pre-buckling well. For $\Gamma_I = 0.65$ the motion can no longer remain within the pre-buckling well and converges to a remote attractor, exhibiting large amplitude cross-well motions. These possible outcomes are rather sensitive to initial conditions and system parameters. So, small variations on these data may lead to different system responses, which may affect the safety of the structure.

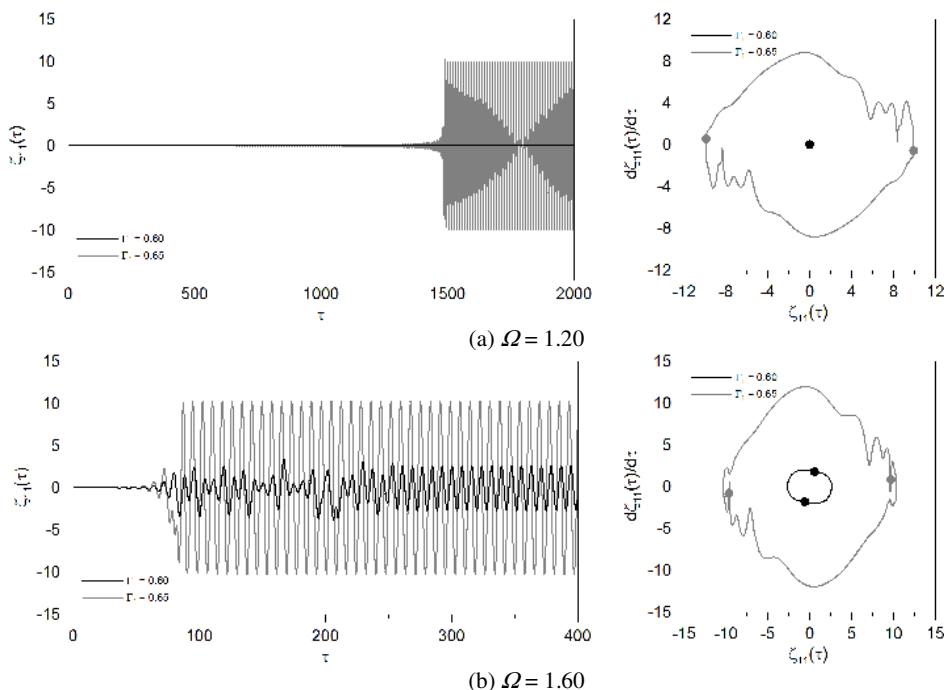


Figure 4. Time responses, phase-portraits and Poincaré maps. ($\Gamma_0 = 0.40$, $G(P_t, \omega, f) = 0$). Sample 3 ($E = 224,87$ GPa) – $Q = 10$.

Figures 5-8 show characteristic bifurcation diagrams of the left and right hand sides of the main parametric instability region. Figures 5 and 7 correspond to sub-critical bifurcations representative of the left hand side of the instability region while Figs. 6 and 8 correspond to super-critical bifurcation representative of the right hand side of the instability region. These bifurcation diagrams are obtained by the brute force method which maps a sequence of stable responses as the bifurcation parameter increases. They are obtained by fixing the forcing frequency and increasing slowly the forcing amplitude.

The black curves are the coordinate $\zeta_{11}(\tau)$ of the Poincaré map of the reference solution obtained with the design values. The gray

curves represent the lower and upper bounds of the coordinate $\zeta_{11}(\tau)$ of the Poincaré map considering the ten different samples. Figures 5 and 6 show the influence of the uncertainties in the value of the Young modulus while Figs. 7 and 8 illustrate the influence of small variations in the shell thickness.

These figures show that small variations in these parameters may lead to significant variations in the critical loads and also in each time response, leading to new bifurcations, as illustrated in Fig. 9, where the bifurcation diagrams obtained for two different values of the Young modulus are presented. Not only variations in the maximum values of the displacements and velocities occur, but also different branches of solutions appear.

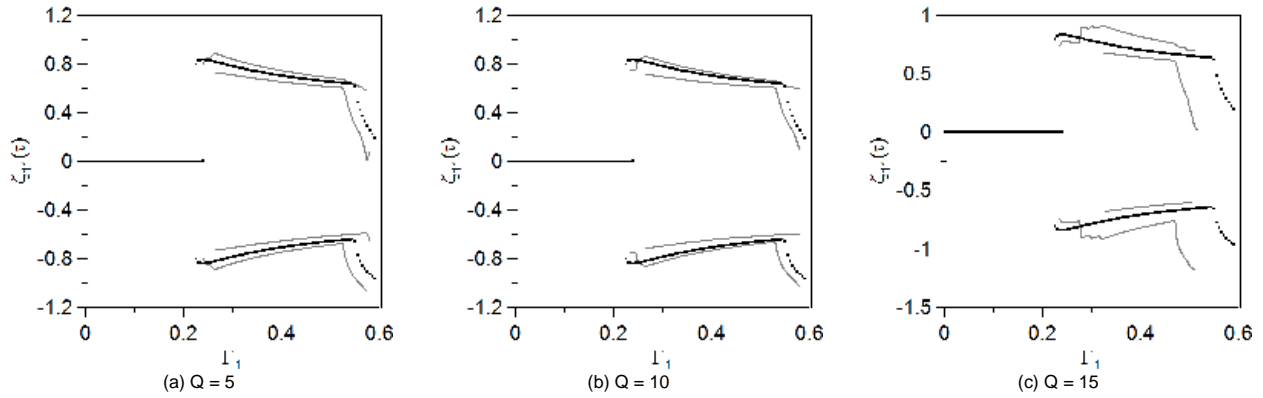


Figure 5. Bifurcation diagram considering an uncertainty in the Young modulus. $\mathcal{I}_0 = 0.40, \Omega = 1.50, G(P_i, \omega, t) = 0$.

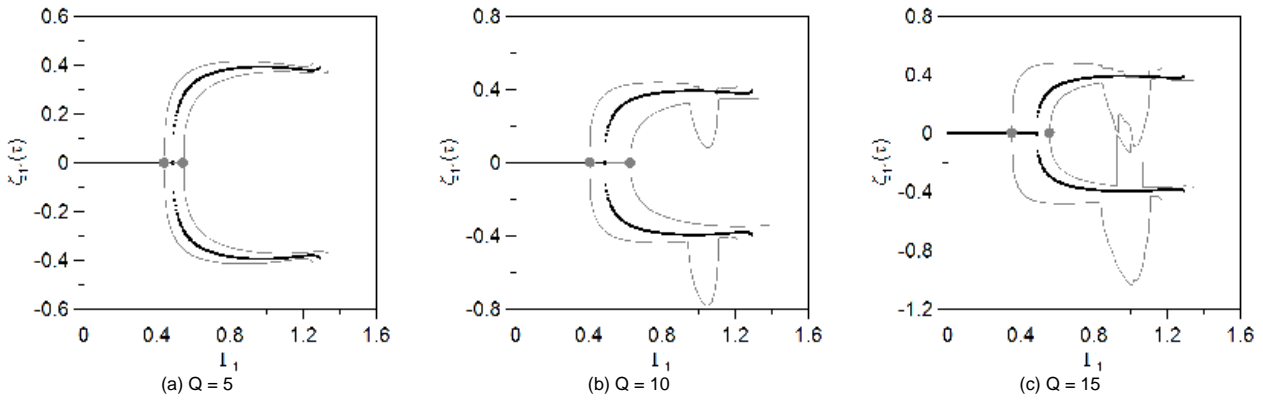


Figure 6. Bifurcation diagram considering an uncertainty in the Young modulus. $\mathcal{I}_0 = 0.40, \Omega = 1.80, G(P_i, \omega, t) = 0$.

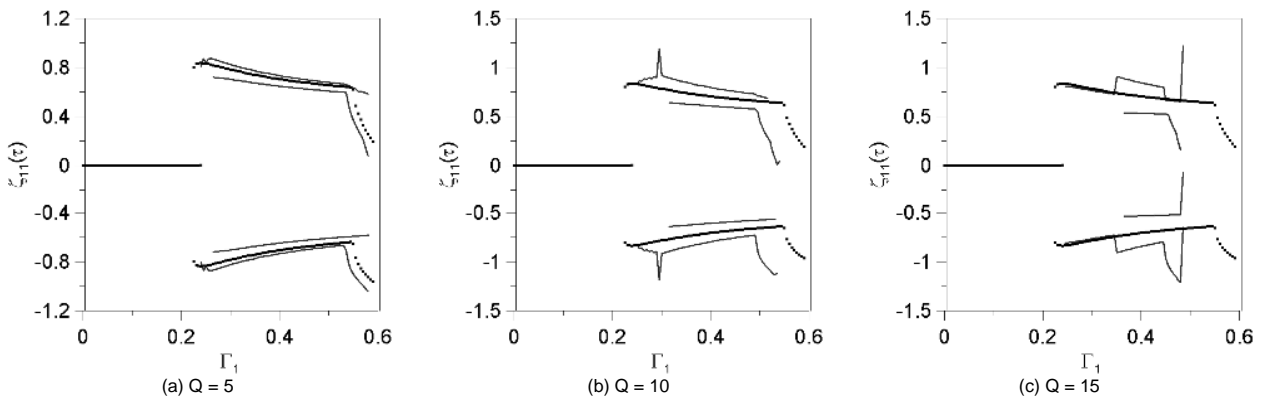


Figure 7. Bifurcation diagram considering an uncertainty in the shell thickness. $\mathcal{I}_0 = 0.40, \Omega = 1.50, G(P_i, \omega, t) = 0$.

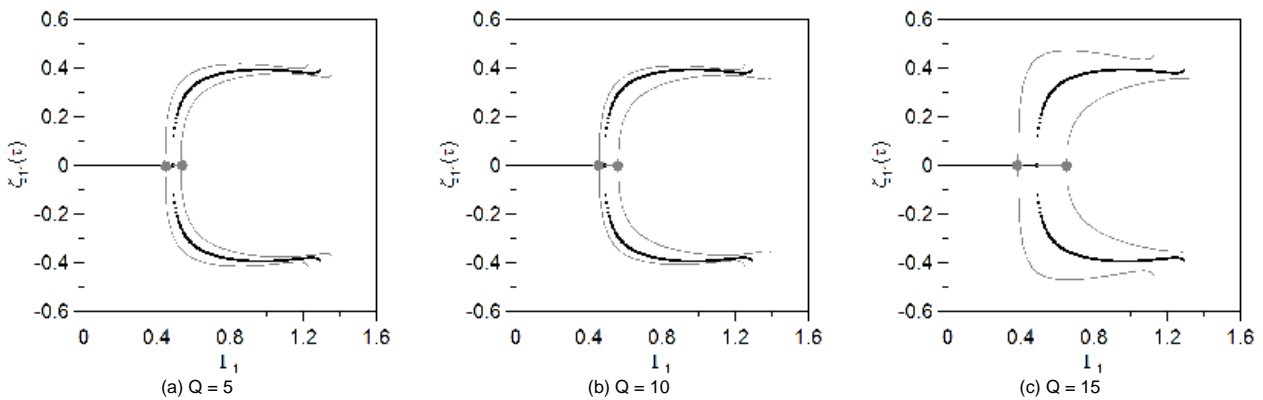


Figure 8. Bifurcation diagram considering an uncertainty in the shell thickness. $\mathcal{I}_0 = 0.40, \Omega = 1.80, G(P_i, \omega, t) = 0$.

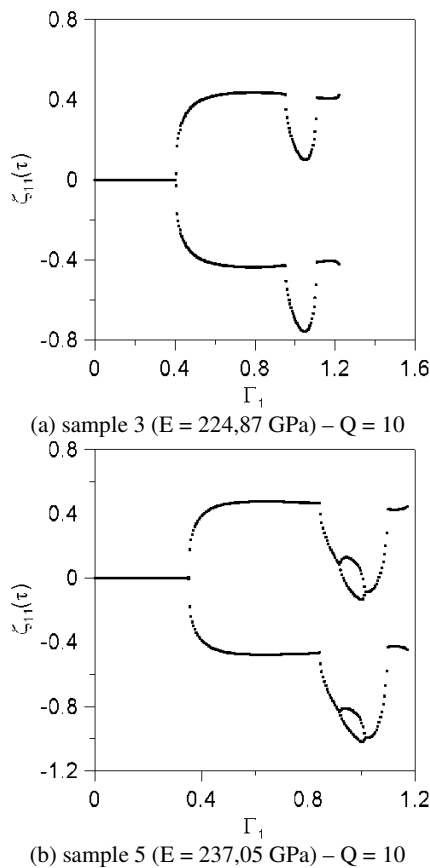


Figure 9. Two samples of the bifurcation diagram considering an uncertainty in Young modulus. $\Gamma_0 = 0.40$, $\Omega = 1.80$, $G(P_i, \omega, t) = 0$.

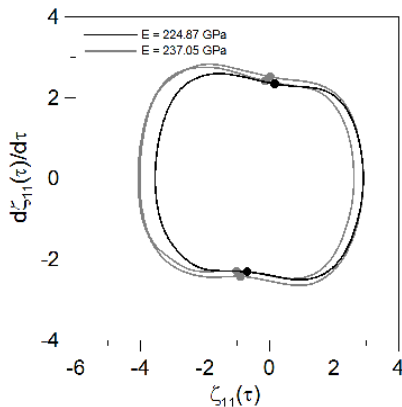


Figure 10. Phase-portrait and Poincaré map for $\Gamma_0 = 0.40$, $\Gamma_1 = 1.00$, $\Omega = 1.80$, $G(P_i, \omega, t) = 0$. Uncertainty in Young modulus.

Figure 10 shows two different shell responses when an uncertainty in Young modulus is considered. While in one case a period two response is observed, in the other the steady state response exhibit a period four times greater than that of the forcing. While the former results from one period doubling bifurcation, the latter is the result of two period doubling bifurcations. This shows that small variations in one parameter may lead to different bifurcation scenarios.

Numerical results with random forces

Figure 11 shows the influence of the random portion of the load, $G(P_i, \omega, t)$, described by Eq. (2), on the parametric instability and escape boundaries of the axially loaded cylindrical shell for one bandwidth, ω_l , 0.50 and two values of the standard deviation parameter, δ , 0.05 and 0.10. For this value of ω_l and δ ten samples are generated and the two critical loads are evaluated, considering the average values of the shell geometry and physical parameters. In Fig. 11, curves in black are the results for a deterministic harmonic force, as shown in Figs. 2 and 3. The dashed gray curves represent the escape load. The presence of noise leads to a dispersion of the results in the right side of the instability region. The continuous gray curves represent the value of the mean load added or subtracted from the value of the standard deviation of ten samples. As the standard deviation parameter, δ , increases, the dispersion of the dynamic buckling loads increase. Also all escape loads of the perturbed system are lower than the permanent escape load of the shell under a deterministic load. So, the shell is sensitive to noise in the excitation and this decreases the safety of the shell in a dynamic environment.

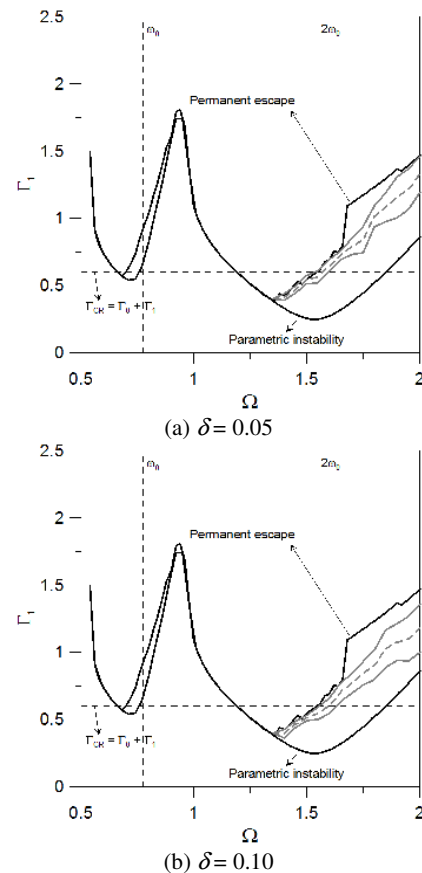


Figure 11. Instability boundaries in force control space. ($\Gamma_0 = 0.40$, $\omega_l = 0.50$).

Figure 12 shows two time responses considering the same set of force parameters ($\Gamma_0 = 0.40$, $\Gamma_1 = 0.675$, $\Omega = 1.60$, $\omega_l = 0.25$, $\delta = 0.10$), but two different random perturbations. As shown in Fig. 12, the escape in these circumstances is indeterminate; the long term response may escape or remain within the pre-buckling well, depending on the external noise, or even escape for a while and return to the pre-buckling well. While the system under

deterministic load displays a sub-harmonic response of period two, the perturbed system exhibit a quasi-periodic motion.

Figure 13 illustrates the characteristic bifurcation diagrams of the main parametric instability region considering $\Gamma_0 = 0.40$, $\omega_l = 0.25$, $\delta = 0.10$. Figure 13a shows a sub-critical bifurcation representative of the shell behavior on the left hand side of the main instability region, while Fig. 13b illustrates the behavior of the shell on the right hand side of the main instability region. The black dots represent the coordinate $\zeta_{11}(\tau)$ of the Poincaré map of the shell

under deterministic harmonic load, while the two gray curves represent the bounds of the coordinates of the Poincaré map obtained after ten samples of the perturbed load (gray dots). The results show that the random small perturbation of the harmonic forcing does not change the overall behavior and bifurcations of the system, causing only small perturbations of the Poincaré map around the fixed points of the deterministic system due to the perturbations of the orbit as illustrated in Fig. 13. The dispersion of points around the fixed points increases as δ increases.

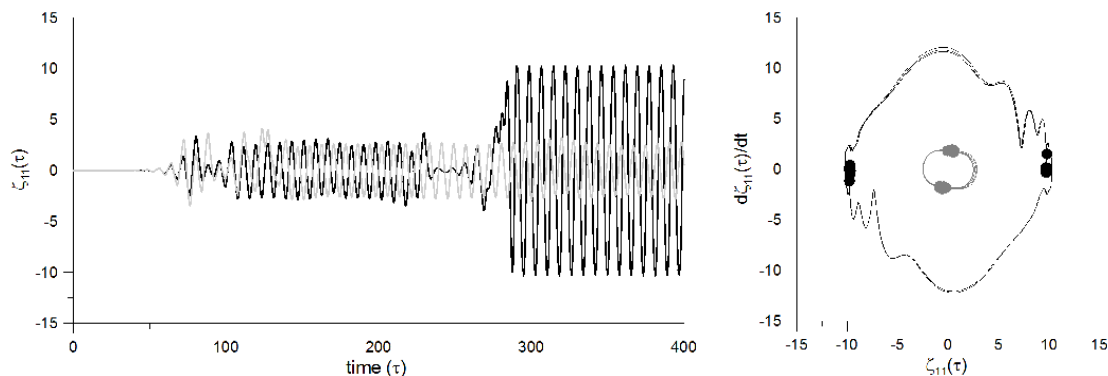


Figure 12. Time response and phase portrait of the cylindrical shell under random noise. ($\Gamma_0 = 0.40$, $\Gamma_1 = 0.675$, $\Omega = 1.60$, $\omega_l = 0.25$, $\delta = 0.10$).

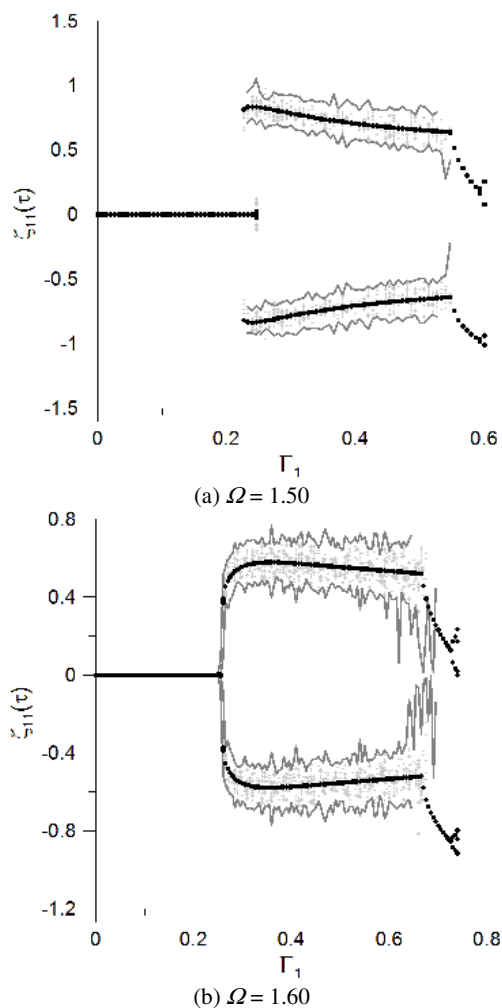


Figure 13. Bifurcation diagrams of the cylindrical shell. ($\Gamma_0 = 0.40$, $\omega_l = 0.25$, $\delta = 0.10$).

Figure 14 illustrates the influence of random noise on the basin of attraction of the shell considering $\Gamma_0 = 0.40$, $\Gamma_1 = 0.40$, $\Omega = 1.60$. It shows three cross-sections of the twelve-dimensional basin of attraction by the $\zeta_{11}(\tau) \times d\zeta_{11}(\tau)/d\tau$ plane. A total of 150×150 cells are considered in the analysis. The black region corresponds to the initial conditions that converge to the period two attractor within the pre-buckling well, while the gray region corresponds to initial conditions that lead to a period two large-amplitude solution outside the pre-buckling well. Figure 14a corresponds to the deterministic case and Fig. 14b and Fig. 14c are related to perturbed solutions obtained with $\delta = 0.05$ and $\delta = 0.10$, respectively, and $\omega_l = 0.25$. In the deterministic case each set of initial conditions leads to a specific attractor. In the non-deterministic case, for each set of initial conditions, the equations of motion are integrated using ten different samples of random perturbation. If in all cases all responses converge to the same attractor as in the deterministic case, the cell is either marked in black or gray, but if they converge to different attractors or if the attractor is different from the one identified in the deterministic case, this means that the response associated with a given set of initial conditions is sensitive to random noise and the cell is marked in white in Fig. 14b and Fig. 14c. As the standard deviation parameter δ increases the white region increases, decreasing the safe region associated with a given attractor.

Figure 15 shows the probability density function of the initial conditions used for the construction of the basins of attraction of Fig. 14. In these figures 22500 sets of initial conditions randomly distributed in the plane $\zeta_{11}(\tau) \times d\zeta_{11}(\tau)/d\tau$ are used and, for each set, the equations of motion are integrated during 400 periods of the harmonic deterministic force. The plane is discretized with 150×150 cells and the number of times that each cell is visited is computed, obtaining in this way a numerical probability density (Kraut, Feudel, and Grebogi, 1999). In the deterministic case, Fig. 15a, sharp peaks are observed in the coordinates corresponding to the fixed points of the small amplitude and large amplitude period two attractors of the basin of attraction depicted in Fig. 15a. As the standard deviation parameter δ and consequently the noise increase, the Poincaré sections show an increasing dispersion of points as illustrated in Fig. 13, which is reflected in the associated probability densities shown in Fig. 15b and Fig. 15c.

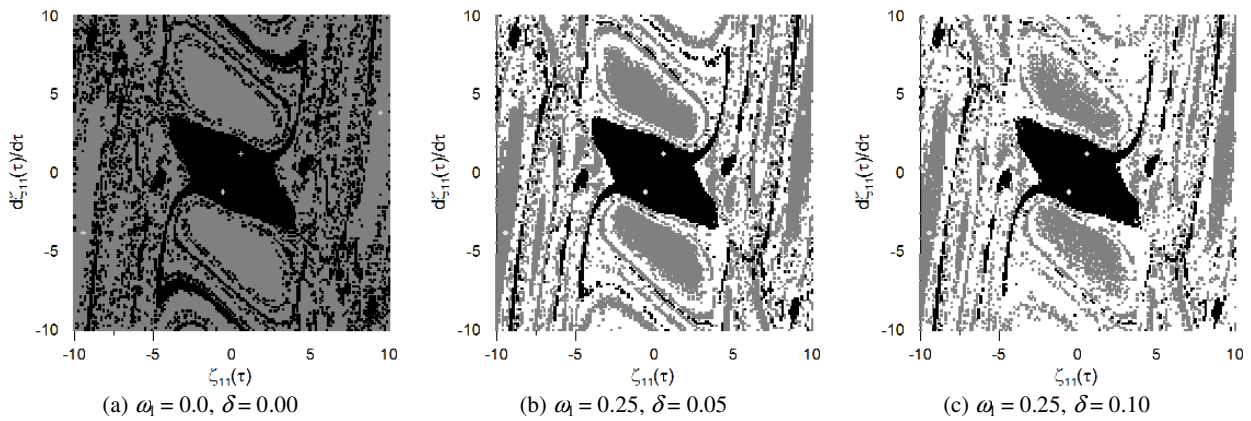


Figure 14. Cross sections of the basin of the attraction of the shell submitted to (a) a deterministic and (b, c) non-deterministic load. ($\Gamma_0 = 0.40$, $\Gamma_1 = 0.40$, $\Omega = 1.60$).

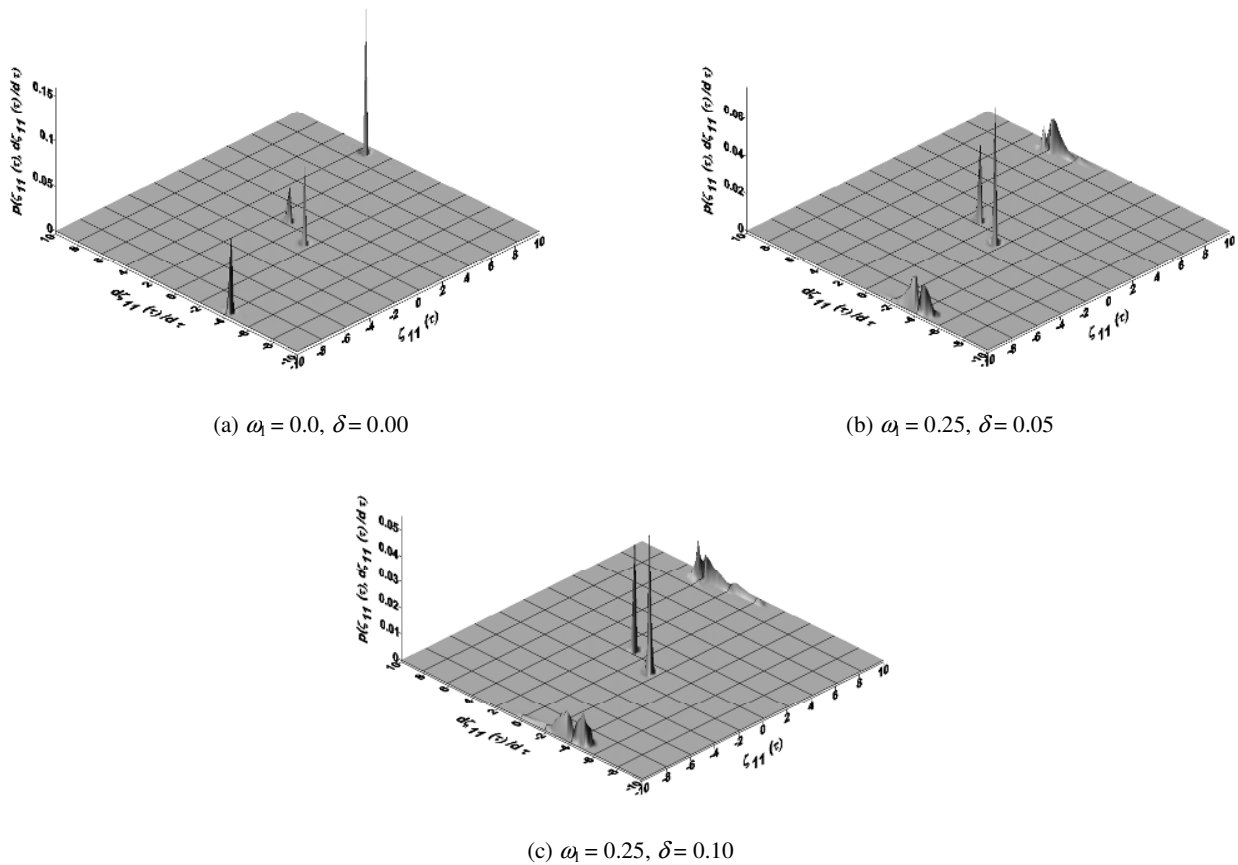


Figure 15. Probability density functions for the set of initial conditions analyzed in Fig. 14. ($\Gamma_0 = 0.40$, $\Gamma_1 = 0.40$, $\Omega = 1.60$).

Conclusions

In this work Donnell’s shallow shell equations are used to study the nonlinear vibrations and instabilities of a simply-supported cylindrical shell. A reduced order model is derived, which satisfies the relevant boundary, continuity and symmetry conditions of the problem and describes with precision the shell motions up to large deflections. The parametric analysis clarifies the influence of small uncertainties of physical parameters and geometry of the shell on the parametric instability and escape

boundaries. Small variations of the physical and/or geometrical parameters lead to a dispersion of the results around the average critical values, in particular variations in the geometrical parameters. This leads to critical loads much lower than the theoretical critical load in some forcing frequency regions, resulting in a decrease in the load carrying capacity, which must be carefully considered at the stage of design. The influence of random noise on the axial load is also investigated. The random noise transforms the n-periodic harmonic responses of the shell into quasi-periodic responses, but does not change the type of

bifurcation connected with the observed instability phenomena, namely, parametric instability and escape from the pre-buckling well. However, in a slowly evolving system the random noise may decrease the escape load in certain excitation frequency ranges. Also, it adds a certain degree of uncertainty to the basin boundaries decreasing the safe region of the shell. The results show that in structures liable do instability, the effect of small uncertainties must be taken into account in the definition of reliable safety factors for design.

Acknowledgements

The authors acknowledge the financial support of the Brazilian research agencies CAPES, CNPq and FAPERJ.

References

- Amabili, M., 2008, "Nonlinear Vibrations and Stability of Shells and Plates", Cambridge University Press, Cambridge, United Kingdom, 374 p.
- Amabili, M. and Paidoussis, M.P., 2003, "Review of studies on geometrically nonlinear vibrations and dynamics of circular cylindrical shells and panels, with and without fluid-structure interaction", *Applied Mechanics Reviews*, Vol. 56, pp. 655-699.
- Batista, R.C. and Gonçalves, P.B., 1994, "Non-Linear Lower Bounds for Shell Buckling Design", *Journal of Constructional Steel Research*, Vol. 29, pp. 101-120.
- Bazant, Z. and Cedolin, L., 1991, "Stability of Structures", Oxford University Press, Oxford, United Kingdom, 1011 p.
- Chu, H.N., 1961, "Influence of large amplitudes on flexural vibrations of a thin circular cylindrical shells", *Journal of Aerospace Science*, Vol. 28, pp. 302-609.
- Evensen, D.A., 1963, "Some observations on the nonlinear vibration of thin cylindrical shells", *AIAA Journal*, Vol. 1, pp. 2857-2858.
- Evensen, D.A., 1967, "Nonlinear flexural vibrations of thin-walled circular cylinders", NASA TN, D-4090.
- Gonçalves, P.B. and Batista, R.C., 1988, "Nonlinear vibration analysis of fluid-filled cylindrical shells", *Journal of Sound and Vibration*, Vol. 127, pp. 133-143.
- Gonçalves, P.B. and Del Prado, Z.J.G.N., 2002, "Nonlinear oscillations and stability of parametrically excited cylindrical shells", *Meccanica*, Vol. 37, pp. 569-597.
- Gonçalves, P.B. and Del Prado, Z.J.G.N., 2005, "Low-dimensional Galerkin model for nonlinear vibration and instability analysis of cylindrical shells", *Nonlinear Dynamics*, Vol. 41, pp. 129-145.
- Gonçalves, P.B. and Santee, D.M., 2008, "Influence of Uncertainties on the Dynamic Buckling Loads of Structures Liable to Asymmetric Post-Buckling Behavior", *Mathematical Problems in Engineering*, Vol. 2008, pp. 1-24.
- Gonçalves, P.B., Silva, F.M.A., and Del Prado, Z.J.G.N., 2008, "Low-dimensional models for the nonlinear vibration analysis of cylindrical shells based on a perturbation procedure and proper orthogonal decomposition", *Journal of Sound and Vibration*, Vol. 315, pp. 641-663.
- Gonçalves, P.B., Silva, F.M.A., Rega, G. and Lenci, S., 2011, "Global dynamics and integrity of a two-dof model of a parametrically excited cylindrical shell", *Nonlinear Dynamics*, Vol. 63, pp. 61-82.
- Koiter, W.T., 1945, "On the stability of elastic equilibrium", PhD dissertation, Delft, Holland.
- Kounandis, A.N., 2006, "Recent advances on postbuckling analyses of thin-walled structures: Beams, frames and cylindrical shells", *Journal of Constructional Steel Research*, Vol. 62, pp. 1101-1115.
- Kraut, S., and Feudel, U., 2002, "Multistability, noise, and attractor hopping: The crucial role of chaotic saddles", *Physical Review E – Rapid Communications*, Vol. 66, pp. 1-4.
- Kraut, S., Feudel, U., and Grebogi, C., 1999, "Preference of attractors in noisy multistable systems", *Physical Review E*, Vol. 59, pp. 5253-5260.
- Kriegesmann, B., Rolfes, R., Hühne, C., Teßmer, J., and Arboez, J., 2010, "Probabilistic design of axially compressed composite cylinders with geometric and loading imperfections", *International Journal of Structural Stability and Dynamics*, Vol. 10, pp. 623-644.
- Lai, Y-C., and Winslow, R.L., 1994, "Fractal basin boundaries in coupled map lattices", *Physical Review E*, Vol. 50, pp. 3470-3473.
- Nowinski, J.L., 1963, "Nonlinear transverse vibration of orthotropic cylindrical shells", *AIAA Journal*, Vol. 1, pp. 617-620.
- Olson, M.D., 1965, "Some experimental observations on the nonlinear vibrations of cylindrical shells", *AIAA Journal*, Vol. 3, pp. 1775-1777.
- Papadopoulos, V. and Papadrakakis, M., 2005, "The effect of material and thickness variability on the buckling load of shells with random initial imperfections", *Computer Methods in Applied Mechanics and Engineering*, Vol. 194, pp. 1405-1426.
- Rega, G. and Lenci, S., 2005, "Identifying, evaluating and controlling dynamical integrity measures in non-linear mechanical oscillators", *Nonlinear Analysis*, Vol. 63, pp. 902-914.
- Santee, D.M., 1999, "Non-linear vibrations and instabilities of imperfection-sensitive structural elements", D. Sc. Thesis, Civil Engineering Department, Catholic University, PUC-Rio, Rio de Janeiro, Brazil, 250 p.
- Silva, F.M.A., Gonçalves, P.B., and Del prado, Z.J.G.N., 2011, "An alternative procedure for the non-linear vibration analysis of fluid-filled cylindrical shells", *Nonlinear Dynamics*, Vol. 66, pp. 303-333.
- Singh, B.N, Yadav, D. and Iyengar, N.G.R., 2002, "Free vibration of composite cylindrical panels with random material properties", *Composite Structures*, Vol. 58, pp. 435-442.
- Soliman, M.S. and Thompson, J.M.T., 1989, "Integrity measures quantifying the erosion of smooth and fractal basins of attraction", *Journal of Sound and Vibration*, Vol. 135, pp. 453-475.
- Soliman, M.S. and Thompson, J.M.T., 1992, "Global Dynamics Underlying Sharp Basin Erosion in Nonlinear Driven Oscillators", *Physical Review A*, Vol. 45, pp. 3425-3431.
- Stefanou, G., 2011, "Response variability of cylindrical shells with stochastic non-Gaussian material and geometric properties", *Engineering Structures*, Vol. 33, pp. 2621-2627.
- Stefanou, G., and Papadrakakis, M., 2004, "Stochastic finite element analysis of shells with combined random material and geometric properties", *Computer Methods in Applied Mechanics and Engineering*, Vol. 193, pp. 139-160.
- Thompson, J.M.T., 1989, "Chaotic behavior triggering the escape from a potential well," *Proceedings of Royal Society London A*, Vol. 421, pp. 195-225.
- Virgin, L.N., 2000, "Introduction to Experimental Nonlinear Dynamics", Cambridge University Press, Cambridge, United Kingdom, 256 p.
- Yadav, D. and Verma, N., 2001, "Free vibration of composite circular cylindrical shells with random material properties. Part II: Applications", *Composite Structures*, Vol. 51, pp. 371-380.
- Ziemian, R.D., 2010, "Guide to Stability Design Criteria for Metal Structures", John Wiley & Sons, Hoboken, New Jersey, USA, 1078 p.